JACS
JOURNAL OF THE AMERICAN CHEMICAL SOCIETY

Communication

pubs.acs.org/JACS

Correlated Electrochemical and Optical Tracking of Discrete Collision Events

Stephen E. Fosdick, Morgan J. Anderson, Elizabeth G. Nettleton, and Richard M. Crooks*

Department of Chemistry and Biochemistry and the Center for Nano- and Molecular Science and Technology, The University of Texas at Austin, 105 East 24th Street, Stop A5300, Austin, Texas 78712-1224, United States

Supporting Information

ABSTRACT: Optical tracking of collisions between insulating microbeads and an ultramicroelectrode surface are correlated to electrochemical measurements and 3D simulations. The experiments are based on partial blocking of the electrode surface by the beads. Results obtained using these three methods provide details regarding the radial distribution of landing locations, the extent of current blockage, collision frequency, motion of beads on the electrode surface following collisions, and aggregation behavior both prior to collisions and afterward on the electrode surface.

Here we report simultaneous electrochemical and optical detection of individual, fluorescent microbeads interacting with an ultramicroelectrode (UME). The important new result is that electrochemical signals can be directly correlated to optical observations of single particles colliding with and moving about an electrode surface. To the best of our knowledge, specific interactions of this sort have not previously been visualized. To implement this experiment, an electrochemical cell is configured atop a microscope objective focused on the electrode surface (Scheme 1a). The electrode potential is then adjusted such that electroactive molecules present in solution undergo faradaic reactions. When a fluorescent bead strikes the electrode surface it blocks part of the electroactive area, and this results in a current decrease (Scheme 1b). Because the beads stick to the surface, these current decreases have a stepped appearance (Scheme 1c). Moreover, the magnitude of the steps depends on the landing location of the particles. The results of this study are highly relevant to chemical and biological electrochemical sensing schemes involving single-particle collisions.

Our work is motivated by previous findings from Quinn et al., who reported the chronoamperometric detection of 150 and 500 nm carboxyl-functionalized latex spheres.[1] They found that when such beads collide with and irreversibly adsorb to a 2.5 μm UME, the electroactive surface area is reduced sufficiently to partially block oxidation of ferrocenemethanol (FcMeOH). Each time a sphere struck the surface, a step-like decrease in the current (i_{step}) was observed, and these were proposed to correspond to individual collisions. They also found that lowering the conductivity of the solution led to more frequent collisions due to increased mass transfer arising from electromigration of the negatively charged beads in the vicinity of the electrode. Lemay and co-workers also noted that the magnitude of i_{step} was proportional to the concentration of FcMeOH present in solution. Their work included 2D and 3D finite-element simulations for the approach of an insulating sphere to an active UME.

Scheme 1

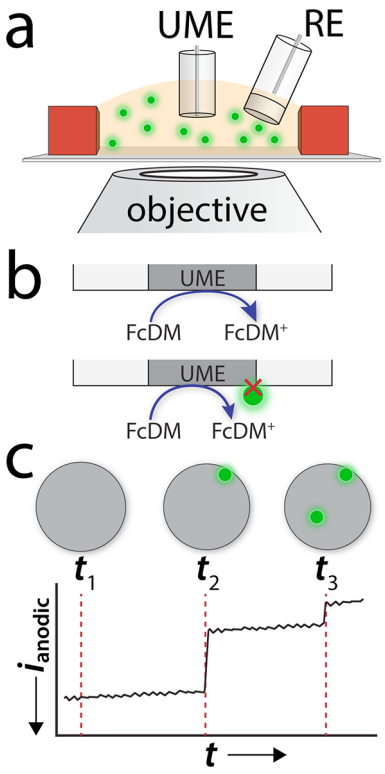

Bard and co-workers extended the foregoing findings by reporting collisions of silica and polystyrene (PS) beads (diameter of 310 and 520 nm, respectively) at Pt UMEs.[2] They described a series of finite-element simulations correlating the effect of the bead landing location with the magnitude of i_{step} as well as the effect of electromigration on the flux of particles to the electrode surface. These simulations predicted that because the diffusive flux of the electroactive species, and thus the electric field, is highest at the edges of the disk UME, the landing position of the beads favors the electrode perimeter over its center. Bard and co-workers also postulated that

Received: February 20, 2013
Published: April 16, 2013

 © 2013 American Chemical Society dx.doi.org/10.1021/ja401864k | J. Am. Chem. Soc. 2013, 135, 5994−5997

occasionally very low current transients might correspond to beads moving and, in some cases aggregating, on the surface of the electrode. Additionally, they employed Poisson statistics to predict the likelihood of aggregates of two or more beads colliding with the electrode surface.

In addition to collisions involving insulating particles, colliding particles can also generate signals through electrocatalytic amplification.[3] Specifically, Bard and Xiao reported single Pt nanoparticle (NP) collisions at UMEs, where the Pt NPs catalyzed H^+ and H_2O_2 reduction at glassy carbon (GC) and Au UMEs, respectively.[4] Compton and co-workers have carried out related experiments, except in their case amplification arises from electrodissolution of Ag NPs.[5] Unwin, Koper, and co-workers used the meniscus formed at the end of a double-barrel micropipet to define an electrochemical cell used to monitor collisions.[6] These groups, and others, have reported many other variants on this same basic experiment over the past few years.[7−20]

Here, we show that it is possible to simultaneously track carboxyl-modified fluorescent PS beads (diameter = 1.03 ± 0.06 μm) using optical microscopy and electrochemical methods. Our experiment is carried out using a 10.0 μm Pt UME immersed in a solution containing the beads, 5.0 mM 1,1′-ferrocenedimethanol (FcDM), and 5.0 mM KNO_3 as a supporting electrolyte (Scheme 1a). When the electrode is held at a potential at which FcDM is oxidized at the mass-transfer-limited rate ($i = i_{lim}$), the negatively charged beads are attracted to the electrode *via* electromigration, and their arrival at the surface of the electrode is monitored both optically and electrochemically.

Experiments were carried out as follows. First, the electrochemical cell was filled with 250 μL of the FcDM + KNO_3 solution in the absence of beads. Cyclic voltammograms and $i-t$ traces were then collected to ensure acceptable noise levels and the value of i_{lim} (Figure S1). Second, 250 μL of a 100 fM bead solution, also containing supporting electrolyte, were injected into the cell, resulting in a final bead concentration of 50 fM. Third, the potential of the UME was stepped from 0 to 0.50 V vs Ag/AgCl, which results in $i = i_{lim}$. The upper left frame of Figure 1a is an optical micrograph of the Pt UME used in this study. The remaining frames in Figure 1a show the collision of each of 10 fluorescent beads with the surface of the UME. These frames were extracted from Movie S1 in the Supporting Information. Figure 1b to 1d are $i-t$ traces that correspond to the optical micrographs, and the numbered current steps are correlated to the numbered micrographs. For example, bead 2 first strikes the electrode about halfway (2.2 μm) along the radius of the UME. It then moves to the outer edge of the electrode at about the same time as bead 3 hits the surface. Beads 7 and 8 appear to oscillate on the surface shortly after colliding, causing a noticeable change in the apparent noise in the $i-t$ trace (Figure 1d). To verify that an oxidation, such as that of FcDM, induces the electromigration (or mass transfer) of negatively charged beads to an active UME, we performed a control experiment where the reduction of *p*-benzoquinone was driven at the UME and no collisions were observed over the course of ∼20 min.

The most interesting result of these experiments is that the locations of bead collisions can be directly correlated to the size of the current step in the $i-t$ trace. To achieve this, the location of each bead is determined using the general approach shown in Figure 2a. Specifically, the centroid of the first bead striking the electrode surface is determined by maintaining a high

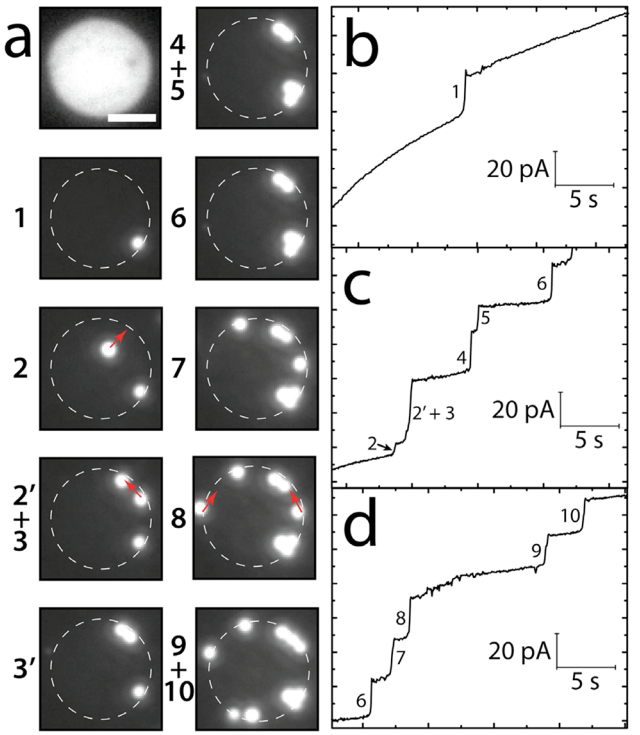

Figure 1. (a) A series of micrographs showing bead collisions at a Pt UME. (Top left) Optical micrograph of the 10 μm Pt UME (the white scale bar indicates 5 μm). The remaining frames show fluorescence micrographs extracted from Movie S1. The numbers to the left of each frame indicate which bead collision is represented in that frame. Arrows have been added to show the motion of the beads on the electrode surface following collisions. (b−d) Chronoamperometric ($i-t$) traces obtained during Movie S1. The time correlated collision from the movie frames (part a) and the $i-t$ traces (parts b−d) are indicated by the numbers in each frame. The current convention used here shows increasing anodic current down, so that collisions cause a decrease in current magnitude from FcDM oxidation (values of i_{step} are positive). Notice that, after beads 7 and 8 collide with the surface, they are observed to move on the surface in the direction of the red arrows. This leads to an increase in the apparent noise between the landing time of beads 8 and 9 in the $i-t$ trace shown in part (d).

intensity of excitation light, which provides sufficient illumination to view the UME. Once the position of the first bead is established relative to the UME, a neutral density filter is inserted into the optical path of the excitation source to reduce the excitation intensity. Next, the positions of subsequent beads colliding with the UME are established relative to the first bead. Figure 2b is a scatter plot showing the measured value of i_{step} vs radial distance of the bead center from the UME center ($r_{b\text{-}e}$) for each of ∼150 bead collisions. Figure S3 shows the results when two-bead aggregates collide with the surface, a result that would be difficult to confirm without the fluorescence data.[2] These data demonstrate that the magnitude of i_{step} depends on the location of the collision of the beads. Larger values of i_{step} are observed for collisions nearer the edge of the electrode than the center. Also, beads tend to collide with greater frequency at the edge of the electrode than at the center (see Figure S4). The frequency of bead collisions decreases with time. Nearly twice as many beads arrive in the first 300 s of the potential step compared to the following 300 s. Another interesting point is that beads colliding on the insulating shroud near the edge of the electrode also cause measurable values of i_{step}, because they still block FcDM flux to the surface of the

dx.doi.org/10.1021/ja401864k | J. Am. Chem. Soc. 2013, 135, 5994−5997

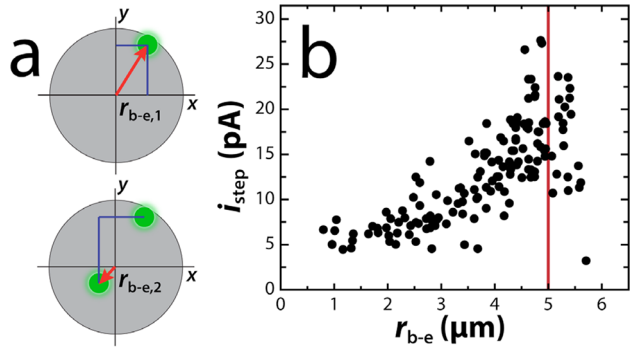

Figure 2. (a) Schematic illustration showing the method used to determine radial bead distance from the UME center ($r_{b\text{-}e}$). The first bead to collide was calibrated against the framework of the UME and the *x*,*y* coordinates (blue lines) converted to radial coordinates (red arrow). The location of subsequent collisions was measured relative to the position of a previously arrived bead, again converting relative differences in *x*,*y* coordinates (blue lines) to radial coordinates (red arrow). (b) Scatter plot of i_{step} vs $r_{b\text{-}e}$ for ∼150 collisions recorded using chronoamperometric and fluorescence data, respectively. Only collisions occurring within the first 600 s of the potential step are shown. The red line indicates the radius of the UME. A plot of i_{step} vs $r_{b\text{-}e}$ for collisions of two-bead aggregates is shown in the Supporting Information (Figure S3).

electrode. This implies that the magnitude of i_{step} is caused not only by blocking portions of the electrode surface but also by other perturbations of the diffusion layer.

In Figure 3a, the results in Figure 2b have been binned into 0.5 μm increments so that they can be directly compared to 3D finite-element simulations. The experimental and simulated results are compared in Figure 3a and are within ∼1.5 pA (∼20%) of one another, which is close to the experimental error given that the baseline noise is on the order of 1 pA peak-to-peak (Figure S1b). Additionally, the distribution of particle sizes also impacts the magnitude of i_{step} for each collision, which contributes to the scatter. An illustration of this point can be found in Figure S8, which shows simulated values of i_{step} for beads of varying diameters. Figure 3b shows the effect of beads centered at several different values of $r_{b\text{-}e}$ on the diffusive flux profile along that radius. This clearly demonstrates why beads at the edge of the disk cause larger values of i_{step}: more FcDM flux is blocked at the edges because a disk UME is not uniformly accessible.[21] Figure 3c−3e are simulated surface plots of the diffusive flux at the disk UME with beads centered at the same $r_{b\text{-}e}$ values as in Figure 3b. Using these types of simulations, it is possible to predict i_{step} for a bead as it moves to different positions on the electrode surface following an initial collision, collision events occurring in close spatial proximity, and collisions of two-bead aggregates, though this level of sophistication is beyond the scope of this initial report. For now, however, we are satisfied that the electrochemical, optical, and theoretical results are in good agreement.

In conclusion, we have used optical tracking and simulations to show that the location of a bead collision on an active UME is related to the magnitude of the resulting current steps. Moreover, details relating to the motion of beads on the electrode surface following collisions, including aggregation behavior, have also been revealed by the optical experiments. Armed with this detailed understanding of insulating collisions, we are ready for future studies aimed at the development of single-particle electrochemical sensing devices.

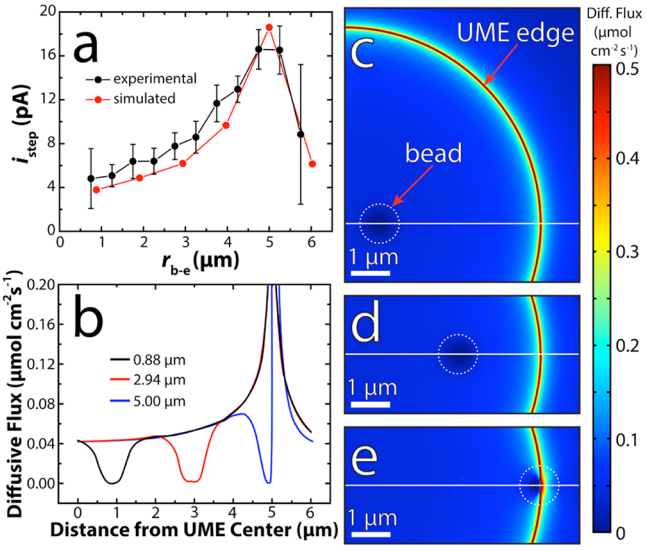

Figure 3. (a) Plot of i_{step} vs $r_{b\text{-}e}$. The black symbols represent data from Figure 2b that were binned into increments of 0.5 μm. The error bars represent the 95% confidence interval for collisions that occurred within the indicated bin. A histogram showing the counts per value bin is included in the Supporting Information (Figure S4). The red circles represent simulated data for the difference in steady-state current at a UME having an insulating spherical particle (1.03 μm) centered at the indicated distance from the center of the UME vs the steady-state current at the bare electrode. (b) Simulated diffusive flux profile across the length of the radius of the UME for different values of $r_{b\text{-}e}$. The maximum flux was 4.2 μmol cm^{-2} s^{-1}, but the color scale was truncated to more clearly show the effect of the insulating beads. (c−e) Surface plots of diffusive flux over a portion of the surface of the UME for $r_{b\text{-}e}$ = 0.88 μm (c), 2.94 μm (d), and 5.00 μm (e). The location of the spheres is indicated by the dashed white circle, and the white line represents the radius of the UME. Details regarding the simulations can be found in the Supporting Information.

■ ASSOCIATED CONTENT

Supporting Information

Information is provided about chemicals and materials, equipment and the experimental setup, description of the finite-element simulations, estimation of D_{FcDM}, a movie from which the results in Figure 1 were extracted, representative electrochemical data, values of i_{step} for two-bead aggregates, histogram of collision events vs distance from the electrode center, correlation of the temporal relationship between the chronoamperometric and optical measurements, bead sizing data, and the simulation parameters. This material is available free of charge via the Internet at http://pubs.acs.org.

■ AUTHOR INFORMATION

Corresponding Author

crooks@cm.utexas.edu

Notes

The authors declare no competing financial interest.

■ ACKNOWLEDGMENTS

We gratefully acknowledge financial support from the U.S. Defense Threat Reduction Agency (Grant No. HDTRA1-11-1-0005). We thank Prof. Allen J. Bard (UT-Austin) for helpful discussions.

REFERENCES

(1) Quinn, B. M.; van 't Ho, P. G.; Lemay, S. G. *J. Am. Chem. Soc.* **2004**, *126*, 8360−8361.
(2) Boika, A.; Thorgaard, S. N.; Bard, A. J. *J. Phys. Chem. B* **2012**, *ASAP*, DOI: 10.1021/jp306934g.
(3) Bard, A. J.; Zhou, H. J.; Kwon, S. J. *Isr. J. Chem.* **2010**, *50*, 267−276.
(4) Xiao, X. Y.; Bard, A. J. *J. Am. Chem. Soc.* **2007**, *129*, 9610−9612.
(5) Zhou, Y.-G.; Rees, N. V.; Compton, R. G. *Angew. Chem., Int. Ed.* **2011**, *50*, 4219−4221.
(6) Kleijn, S. E. F.; Lai, S. C. S.; Miller, T. S.; Yanson, A. I.; Koper, M. T. M.; Unwin, P. R. *J. Am. Chem. Soc.* **2012**, *134*, 18558−18561.
(7) Xiao, X. Y.; Fan, F.-R. F.; Zhou, J. P.; Bard, A. J. *J. Am. Chem. Soc.* **2008**, *130*, 16669−16677.
(8) Xiao, X. Y.; Pan, S. L.; Jang, J. S.; Fan, F.-R. F.; Bard, A. J. *J. Phys. Chem. C* **2009**, *113*, 14978−14982.
(9) Kwon, S. J.; Fan, F.-R. F.; Bard, A. J. *J. Am. Chem. Soc.* **2010**, *132*, 13165−13167.
(10) Zhou, H. J.; Fan, F.-R. F.; Bard, A. J. *J. Phys. Chem. Lett.* **2010**, *1*, 2671−2674.
(11) Kwon, S. J.; Zhou, H.; Fan, F.-R. F.; Vorobyev, V.; Zhang, B.; Bard, A. J. *Phys. Chem. Chem. Phys.* **2011**, *13*, 5394−5402.
(12) Kwon, S. J.; Bard, A. J. *J. Am. Chem. Soc.* **2012**, *134*, 10777−10779.
(13) Kwon, S. J.; Bard, A. J. *J. Am. Chem. Soc.* **2012**, *134*, 7102−7108.
(14) Zhou, H. J.; Park, J. H.; Fan, F.-R. F.; Bard, A. J. *J. Am. Chem. Soc.* **2012**, *134*, 13212−13215.
(15) Zhou, Y.-G.; Rees, N. V.; Compton, R. G. *Chem. Phys. Lett.* **2011**, *511*, 183−186.
(16) Zhou, Y.-G.; Rees, N. V.; Compton, R. G. *ChemPhysChem* **2011**, *12*, 2085−2087.
(17) Zhou, Y.-G.; Stuart, E. J. E.; Pillay, J.; Vilakazi, S.; Tshikhudo, R.; Rees, N. V.; Compton, R. G. *Chem. Phys. Lett.* **2012**, *551*, 68−71.
(18) Zhou, Y.-G.; Rees, N. V.; Compton, R. G. *Chem. Commun.* **2012**, *48*, 2510−2512.
(19) Dasari, R.; Robinson, D. A.; Stevenson, K. J. *J. Am. Chem. Soc.* **2012**, *135*, 570−573.
(20) Alligrant, T. M.; Nettleton, E. G.; Crooks, R. M. *Lab Chip* **2013**, *13*, 349−354.
(21) Bard, A. J.; Faulkner, L. R. *Electrochemical Methods: Fundamentals and Applications*, 2nd ed.; John Wiley & Sons: New York, 2001.